

Photoexcited Coherent Tunneling in a Double-Barrier Superlattice

K. K. Choi, B. F. Levine, C. G. Bethea, J. Walker, and R. J. Malik

AT&T Bell Laboratories, Murray Hill, New Jersey, 07974

(Received 2 July 1987)

We have observed unambiguously the coherent tunneling of photoexcited electrons through an unequal $\text{Al}_x\text{Ga}_{1-x}\text{As}$ double-barrier superlattice structure. This observation confirms the Fabry-Perot quantum-mechanical interference mechanism in this system. On the basis of this result, a high-responsivity infrared photodetector can be designed with low dark current.

PACS numbers: 73.40.Gk, 73.40.Kp

The observation of negative differential resistance¹⁻⁶ in double-barrier tunneling structures intrigues many scientists as a basic example of quantum mechanics. The original idea of Tsu and Esaki¹ is based on the coherent tunneling of a resonant electron which produces interfering Fabry-Perot reflections from the first and second barriers, leading to an overall global unity resonant transmission factor if the two barriers have equal individual transmissions. The time scale for the buildup of this resonance is given by⁵⁻⁹ $\tau_0 = \hbar/\delta E_1 = m^* d^2/\pi \hbar t$, where δE_1 is the lifetime energy width of the ground state in the well, d is the well width, and t is the barrier transmission coefficient. The resonant tunneling condition requires that the perpendicular momentum be unchanged during τ_0 . In the presence of impurity scatterings within the plane of the well, this means τ_0 has to be less than the impurity scattering time τ_e in order for the resonance to be observable. However, for the double-barrier structures usually used in tunneling experiments² τ_0 is estimated to be 3 ps, which is comparable with or even longer than the estimated τ_e (≈ 0.1 ps). These considerations make the distinction between coherent and sequential^{5,10-13} (i.e., two step) tunneling inconclusive.

For ground-state tunneling it is difficult to achieve this coherent condition $\tau_0 < \tau_e$, since reducing τ_0 sufficiently requires barriers so thin that monolayer fluctuations tend to increase the scattering time significantly. For photoexcited tunneling,¹⁴⁻¹⁶ however, t can be large (and hence τ_0 small) because of the low effective barrier height of the excited state; hence, coherent tunneling can be observed.

In this Letter we describe the unambiguous observation of this photoexcited coherent tunneling in an unsymmetrical double-barrier superlattice. The band structure for this superlattice is shown in Fig. 1. The sample was grown by molecular-beam epitaxy and consists of fifty periods of 72-Å GaAs quantum wells (doped $n = 1.0 \times 10^{18} \text{ cm}^{-3}$), 39-Å undoped $\text{Al}_{0.33}\text{Ga}_{0.67}\text{As}$, 18-Å undoped GaAs, and 154-Å undoped $\text{Al}_{0.33}\text{Ga}_{0.67}\text{As}$. The quantum wells are sandwiched between the top (0.5 μm) and bottom (1 μm) GaAs contact layers with $n = 1 \times 10^{18} \text{ cm}^{-3}$. The band diagram is shown in Fig. 1(a). In this structure, each period consists of a thicker

well (W_1), a thinner well (W_2), a thicker barrier (B_1), and a thinner barrier (B_2). For the uncoupled wells, there are two states ($E_1 = 47 \text{ meV}$, $E_2 = 183 \text{ meV}$) in W_1 , and only one state ($E'_1 = 174 \text{ meV}$) in W_2 . For the electrons in W_1 with energy E_1 , the global transmission T_{seq} for the two barriers is $t_1(E_1)t_2(E_1)$ where t_1 and t_2 are the individual transmissions for B_1 and B_2 , respectively. Since t_1 is very small ($\delta E_1 \approx 10^{-4} \text{ meV}$), its field dependence dominates the conduction.

When an electric field is present, the superlattice structure is broken up into high-field domains and low-field domains.^{12,13} In both regimes, electron transport out of E_1 is via sequential tunneling. However, if one photoexcites electrons from E_1 to the excited state close to E_2 , the conduction mechanism of the photoexcited

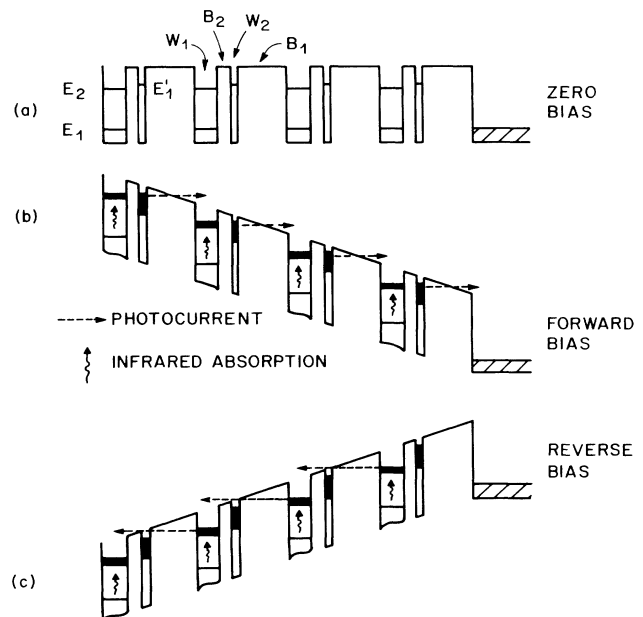


FIG. 1. (a) The energy-band diagram of the structure. In this structure, only the wide well is doped. (b) The band diagram under forward bias. The shaded area indicates the lifetime width of the state. (c) The band diagram under reverse bias.

electrons can be quite different. In the high-field domain (under forward bias) where E_1 is approximately aligned with E_2 of the adjacent period [Fig. 1(b)], the lifetime width ($\Delta E_1'$) of the state in W_2 can be large (>50 meV) compared with impurity broadening (≈ 7.4 meV) because of the large $t_1(E_1')$ and $t_2(E_1')$ at high field. In this case, the coherent tunneling of the photoexcited electron from W_1 through the state E_1' and out of the barriers is possible. In addition, $t_1(E_1')$, originally smaller than $t_2(E_2)$ at zero bias, increases more rapidly under an applied field, finally becoming greater than $t_2(E_2)$ at large bias. Therefore, in a certain range of applied voltage, $t_1(E_1') \approx t_2(E_2)$ and a large coherent resonant enhancement is expected. This is in contrast to the case of reverse bias [Fig. 1(c)], in which $t_1(E_2)$ is always much smaller than $t_2(E_1')$. In order to study the system quantitatively, we use the WKB approximation for coherent tunneling and obtain the result

$$T_{\text{coh}}(E) = 4 \left[\left(\frac{t_1}{t_2} + \frac{t_2}{t_1} \right) \cos^2 \theta + \left(\frac{t_1 t_2}{16} + \frac{16}{t_1 t_2} \right) \sin^2 \theta + 2 \right]^{-1}, \quad (1)$$

where $\theta = (2m^*)^{1/2} W_2 [E^{1/2} - (E_1')^{1/2}] / \hbar$ is the phase angle measured relative to the angle at the resonance energy. At small biases, $t_1(E)$ and $t_2(E)$ are both small so that the WKB approximation for the trapezoidal barriers can be used. At larger biases where the barriers become triangular, the numerical solution using Airy functions is employed.¹⁷ In Fig. 2, we plot T_{coh} for forward (T_{coh}^f)

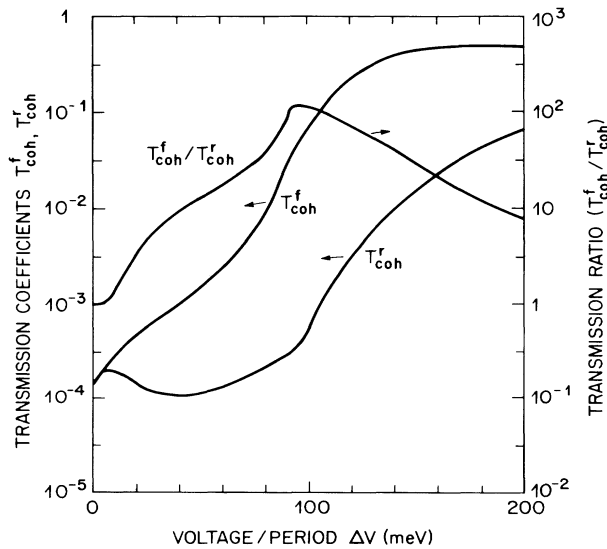


FIG. 2. The theoretical values of the transmission coefficients vs voltage drop per period ΔV under forward bias (T_{coh}^f) and reverse bias (T_{coh}^r) and their ratio on the assumption of coherent tunneling.

and reverse (T_{coh}^r) bias (at $E = 170$ meV measured from the center of W_1) as a function of the voltage drop across a period ΔV . Note that their ratio starts from unity at small bias and rapidly increases to ≈ 100 at $\Delta V = 100$ meV, and then falls back to ≈ 8 at large bias. In contrast, if sequential tunneling were the dominant mechanism, the maximum forward-to-reverse transmission ratio would only be 10. Hence, by measuring the voltage dependence of the photoresponse of the device and its ratio between the forward and reverse bias, one can differentiate between coherent tunneling and sequential tunneling.

In order to measure the photocurrent, the substrate is polished at a 45° angle as described previously,¹⁴⁻¹⁶ and the infrared radiation of $\lambda = 10.3 \mu\text{m}$ (corresponding to the energy used in calculating Fig. 2) is incident on this face. All the measurements were performed at $T = 15$ K with a device having an area of $3 \times 10^{-4} \text{ cm}^2$. The dark current versus voltage characteristics are similar for both polarities (Fig. 3), except for the structure near 6 V in forward bias. This structure is due to the formation¹⁵ of a new even higher field domain (beyond the E_1 and E_2 alignment) as a result of the resonance of E_1 with the lowest continuum resonance E_3 (above the quantum well).¹⁸ (This polarity difference may be due to the growth asymmetry in the two GaAs- $\text{Al}_x\text{Ga}_{1-x}\text{As}$ heterointerfaces.)

Figure 4 shows the responsivity of the device, $R = I_s/P_0$, where I_s is the photocurrent and P_0 is the incident light power. Below 5 V, R in forward bias (R_f) is 2 orders of magnitude larger than R in reverse bias (R_r). At higher voltage, they approach each other, consistent with

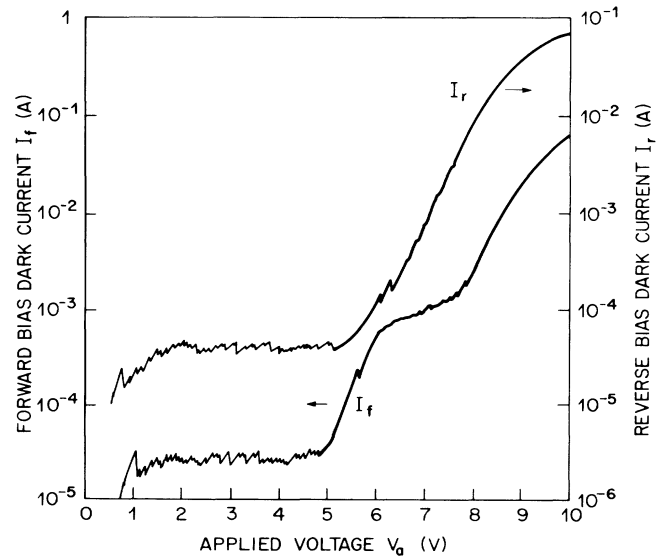


FIG. 3. The dark-current characteristics under forward bias (I_f) and reverse bias (I_r) at different applied voltages (V_a). The area of the device is $3 \times 10^{-4} \text{ cm}^2$. (Note the scale change in the I_f and I_r axes.)

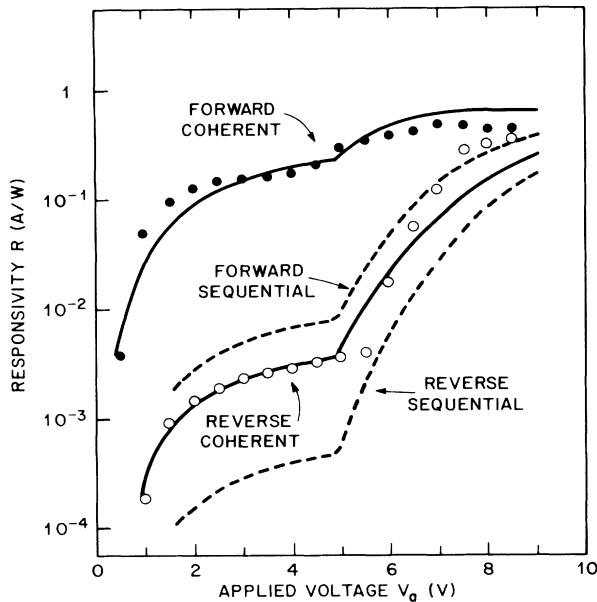


FIG. 4. The experimental result of the responsivity (R) in forward bias (filled circles) and reverse bias (open circles), and theory with the assumptions of coherent tunneling (solid curves) under forward bias T_{coh}^f and reverse bias T_{coh}^r and of sequential tunneling (dashed curves) under forward bias T_{seq}^f and reverse bias T_{seq}^r .

the theory of coherent tunneling. In order to demonstrate this, we can calculate R_f using¹⁴⁻¹⁶

$$R_f = \frac{e\alpha}{h\nu} \frac{1}{m} \sum_{x=1}^m (e^{-ax} + e^{-a(100-x)}) \times p_f(x) L(x) (1 - e^{-x/L(x)}), \quad (2)$$

$$p_f(x) = [1 + 2d/\tau^* v_p T_{\text{coh}}^f(x)]^{-1}, \quad (3)$$

$$L(x) = \Delta V(x) / [\Delta E - \Delta V(x)], \quad (4)$$

where $\alpha = 770 \text{ cm}^{-1}$ is the absorption coefficient, $h\nu$ is the photon energy, x is the superlattice period index, m is the number of high-field domains, $p_f(x)$ is the photoexcited tunneling escape probability, $L(x)$ is the hot-electron mean free path after tunneling out of the well, $\tau^* \approx 100 \text{ fs}$ (Refs. 14-16) is the effective excited-state recombination lifetime, v_p is the electron phase velocity in state E_2 , and ΔE is the photoexcited hot-electron energy relaxation per period.¹⁴⁻¹⁶ For reverse bias, R_r is given by Eq. (2) but with T_{coh}^f replaced by T_{coh}^r and x replaced by $50 - x$ in the light-absorption terms.

The responsivity depends on the potential profile of the superlattice at each bias, which can be deduced from the dark-current characteristics.¹⁵ For applied bias voltages between the values $0.75 \text{ V} \leq V_a \leq 5 \text{ V}$ (from Fig. 3), the superlattice is broken into low-field domains and high-field domains.^{12,14-16} In the low-field domains, the voltage drop is $\approx 7 \text{ mV}$ per period,¹² while in the high-field

domains, the voltage drop is 93 mV per period. (Since the high-field-domain formation quantizes the voltage drop per period, the difference in T_{coh}^f and T_{coh}^r below 93 mV in Fig. 2 is not observable in our experiment.) Beyond 5 V , the forward-bias I - V characteristic is different from that for reverse bias, because of the formation of even higher field domains as discussed above.

To calculate the responsivity we determine the spatial dependence of the potential drop $V(x)$ as previously,^{12,14-16} using the same simple potential profile for both the forward and reverse biases, in order not to obscure the important basic physics of the asymmetrical tunneling transport which only depends weakly on the details of $V(x)$. Combining this with Eqs. (2)-(4), and using $\Delta E \approx 95 \text{ meV/period}$ as a fitting parameter, we achieve good agreement between the coherent tunneling theory and experiment for both polarities (Fig. 4). (It should be noted that ΔE primarily determines the magnitude of R , not its shape.) The slight discrepancy in T_{coh}^r may be due to our neglect of the weak reflection of the second interface of the thick barrier.¹⁹ In strong contrast, if we assume sequential tunneling instead [$T_{\text{coh}}^f(x)$ is replaced by $T_{\text{seq}} = t_1 t_2$ in Eq. (3)], the theoretical predictions (dashed line in Fig. 4) will be an order of magnitude lower than the experimental data and also have a totally different voltage dependence. Therefore, we conclude that the photoexcited electrons tunnel out of the wells coherently (i.e., Fabry-Perot reflection interferences are important) even though the dark current is transported via sequential tunneling.

In conclusion, we have demonstrated that, under suitable conditions, coherent tunneling can be observed and unambiguously differentiated from sequential tunneling. This device not only demonstrates interesting physics of fundamental interest, but also provides a very useful concept in the design of a high-responsivity, low dark-current, $10\text{-}\mu\text{m}$ infrared photodetector. The present device has a responsivity of $R = 0.3 \text{ A/W}$ at $V_a = 5 \text{ V}$ due to the low absorption coefficient²⁰ at $\lambda = 10.3 \mu\text{m}$ which is 6 times smaller than usual.^{21,22} Thus, a more appropriate measure of the intrinsic responsivity is $R \approx 2 \text{ A/W}$ which is comparable to our previous best result. In addition, the dark current for this double-barrier superlattice detector is over 2 orders of magnitude lower than that achieved with simple square tunneling barriers.^{14-16,23} This new structure, therefore, has the same high responsivity but with a much lower dark current, and hence appears particularly promising for high-sensitivity detectors. Similar improvements should be obtainable by the use of barriers which are thin at the top and thick at the bottom (e.g., triangular or stepped-thickness barriers).

¹R. Tsu and L. Esaki, Appl. Phys. Lett. **22**, 562 (1973).

- ²T. C. L. G. Sollner, W. D. Goodhue, P. E. Tannenwald, C. D. Parker, and D. D. Peck, *Appl. Phys. Lett.* **43**, 588 (1983).
- ³T. Shewchuk, P. C. Chopin, P. D. Coleman, W. Kopp, R. Fischer, and H. Morkoc, *Appl. Phys. Lett.* **46**, 508 (1985).
- ⁴M. Tsuchiya and H. Sakaki, *Jpn. J. Appl. Phys. Pt. 1* **25**, 185 (1986), and *Appl. Phys. Lett.* **50**, 1503 (1987).
- ⁵F. Capasso, K. Mohammed, and A. Y. Cho, *IEEE J. Quantum Electron.* **22**, 1853 (1986).
- ⁶B. Ricco and M. Ya. Azbel, *Phys. Rev. B* **29**, 1970 (1984).
- ⁷A. D. Stone and P. A. Lee, *Phys. Rev. Lett.* **54**, 1196 (1985).
- ⁸P. J. Price, *Superlattices Microstruct.* **2**, 593 (1986).
- ⁹N. Harada and S. Kuroda, *Jpn. J. Appl. Phys. Pt. 2* **25**, L871 (1986).
- ¹⁰S. Luryi, *Appl. Phys. Lett.* **47**, 490 (1985).
- ¹¹H. Morkoc, J. Chen, U. K. Reddy, and T. Henderson, *Appl. Phys. Lett.* **49**, 70 (1986).
- ¹²K. K. Choi, B. F. Levine, R. J. Malik, J. Walker, and C. G. Bethea, *Phys. Rev. B* **35**, 4172 (1987).
- ¹³L. Esaki and L. L. Chang, *Phys. Rev. Lett.* **33**, 495 (1974).
- ¹⁴B. F. Levine, K. K. Choi, C. G. Bethea, J. Walker, and R. J. Malik, *Appl. Phys. Lett.* **50**, 1092 (1987).
- ¹⁵K. K. Choi, B. F. Levine, C. G. Bethea, J. Walker, and R. J. Malik, *Appl. Phys. Lett.* **50**, 1814 (1987).
- ¹⁶B. F. Levine, K. K. Choi, C. G. Bethea, J. Walker, and R. J. Malik, *Appl. Phys. Lett.* **51**, 934 (1987).
- ¹⁷S. L. Chuang and K. Hess, *J. Appl. Phys.* **61**, 1510 (1987).
- ¹⁸M. Heiblum, in *High Speed Electronics*, edited by B. Källbäck and H. Beneking (Springer-Verlag, Berlin, 1986).
- ¹⁹T. W. Hickmott, P. M. Solomon, R. Fischer, and H. Morkoc, *Appl. Phys. Lett.* **44**, 90 (1984).
- ²⁰This is due to a somewhat lower doping density in the wells, and the peak intersubband absorption being at $\lambda = 9.1 \mu\text{m}$ rather than at the measuring wavelength $\lambda = 10.3 \mu\text{m}$.
- ²¹B. F. Levine, R. J. Malik, J. Walker, K. K. Choi, C. G. Bethea, D. A. Kleinman, and J. M. Vandenberg, *Appl. Phys. Lett.* **50**, 273 (1987).
- ²²L. C. West and S. J. Eglash, *Appl. Phys. Lett.* **46**, 1156 (1985).
- ²³The device measured in Ref. 15 has a dark current of 200 μA for a 50- μm -diam mesa at a bias for which $R \approx 2 \text{ A/W}$. The present 200- μm -diam device would have a dark current of only 1 μA for this same diameter.